ELSEVIER

Surface and Coatings Technology 146–147 (2001) 152–161

SURFACE & COATINGS TECHNOLOGY

www.elsevier.com/locate/surfcoat

As-deposited mixed zone in thermally grown oxide beneath a thermal barrier coating

K.S. Murphy[a,*], K.L. More[b], M.J. Lance[b]

[a]*Howmet Research Corporation — Howmet Castings, an Alcoa Business, 1500 S. Warner Street, Whitehall, MI 49461, USA*
[b]*Oak Ridge National Laboratory, P.O. Box 2008, Oak Ridge, TN 37831-6068, USA*

Abstract

Gas turbine designers are increasingly using electron-beam physical vapor deposited (EB-PVD) thermal barrier coatings (TBC) to meet the challenge of higher efficiency gas turbine engine requirements. A key feature for expanding the use of TBCs is increased spallation life and reduced spallation life variability. Such a coating system comprises a substrate (Ni-based single crystal alloy), a bond coat (diffusion aluminide or MCrAlY), a ceramic (7 wt.% yttria stabilized zirconia), and a thin thermally grown oxide (TGO) between the bond coat and the ceramic. The TGO is intended to be α-alumina, but evidence reported by other researchers suggests that in some cases the as-deposited TGO may not be entirely α-alumina. The thin nature of the TGO in as-deposited TBCs (<0.5 μm) makes analysis of the phases present and morphology difficult. Advancements in transmission electron microscopy (TEM) sample preparation and photo-stimulated luminescence spectroscopy (PSLS) have allowed higher quality and easier characterization of the TGO. In this study, EB-PVD TBCs were applied to platinum–aluminide bond coats on a Ni-based superalloy. Three types of coatings were produced by changing one PVD process variable. The as-processed TGO layer was characterized utilizing scanning transmission electron microscopy (STEM) and PSLS for each of the three coating process variables used. Results of this work found that the TGO comprised two sublayers; (1) a continuous layer of γ-Al_2O_3 between the mixed oxide zone and the bond coat; and (2) a mixed oxide zone between the continuous γ-Al_2O_3 and the TBC layer. An explanation for the creation of the mixed oxide zone found in these TGO morphologies is presented. © 2001 Elsevier Science B.V. All rights reserved.

Keywords: Phase transitions; Transmission electron microscopy; Electron beam evaporation; Pack diffusion coatings; Zirconium oxide; Thermally grown oxide

1. Introduction

Advances in gas turbine efficiency are related to turbine inlet temperature increases allowed by component materials, design and thermal resistance. The increased efficiency can be in the form of greater component durability, greater component performance, or a combination thereof. A key feature for expanding the use of thermal barrier coatings (TBCs) is increased spallation life and reduced spallation life variability.

TBCs have been used in gas turbines for a number of decades [1]. The initial TBCs were applied by plasma spray deposition in air. Improvement in bond coat technology allowed TBC usage to move from protecting sheet metal components in the rear of the turbine to use on turbine vanes [2] and combustor components. Changing the deposition method from plasma spray to electron beam physical vapor deposition (EB-PVD) methods has allowed TBC use on turbine blades [2].

The main reasons EB-PVD TBCs have been successful on turbine components is the columnar ceramic morphology unique to EB-PVD deposition and the surface qualities attainable with this process. The segmented columnar morphology accommodates the thermal expansion mismatch between the metallic component and the ceramic better than the porosity and micro-cracking used in plasma sprayed TBCs. The columns are relatively dense and allow the ceramic to

* Corresponding author. Tel.: +1-231-894-7954; fax: +1-231-894-7826.
E-mail address: kmurphy@howmet.com (K.S. Murphy).

0257-8972/01/$ - see front matter © 2001 Elsevier Science B.V. All rights reserved.
PII: S0257-8972(01)01371-8

resist erosion in the high velocity gas turbine environment better than plasma sprayed coatings [3,4]. The EB-PVD surface morphology is relatively smooth as compared to plasma sprayed TBCs and can be easily polished to attain a finish of 0.76 μm (30 micro-inches). Since the coating forms from a vapor phase, the coating process does not easily block cooling holes. Holes as small as 0.254 mm (10 mils) can be coated without bridging the hole opening and coating constriction, or coat-down, of the hole is repeatable.

Early descriptions of the EB-PVD system identified the substrate, the bond coat, the columnar ceramic, and an alumina layer between the bond coat and the ceramic [5,6]. Strangman intended the alumina layer to be α-alumina, which could be thermally grown or deposited onto the surface of the bond coat. The most common method in use is thermally grown, hence the use of TGO to describe this layer. Failure of this system occurs in the vicinity of the TGO [2]; usually between the TGO and the TBC or between the TGO and the bond coat. Consequently, improvement in EB-PVD TBC spallation life will come from greater understanding of the TGO and its interaction with the TBC and bond coat.

Transmission electron microscopy (TEM) work has shown that meta-stable phases of alumina may also exist in the TGO [7]. Pioneering work by Clarke et al. [8–11] uses photo-stimulated luminescence spectroscopy (PSLS) to measure stress state and phases in the TGO non-destructively through the TBC. After short times at use temperatures, the TGO on β-phase (Ni,Pt)Al bond coats converts entirely to α-alumina.

The purpose of this work is to study the TGO region in the as-deposited TBC deposited condition. Thermally grown oxide thickness is on the order of 0.5 μm or less in as-deposited TBCs. Consequently, TEM is necessary to study the TGO morphology and crystallographic structure. Preparation of suitable TEM specimens from these bulk samples, having all the necessary layers and interfaces sufficiently thin and intact for TEM/STEM analysis, has long been a problem. Recently, the focused ion beam (FIB) technique has been used to make uniformly thin samples of these and other traditionally difficult-to-prepare materials [12]. Large, intact thin areas through the TBC/TGO/(Ni,Pt)Al layers are produced using the FIB, enabling direct imaging of the full TGO. TEM analysis, combined with bulk, non-destructive evaluation via PSLS, have been used to fully characterize the TGO microstructure and phase make-up as a function of coating process in this work.

2. Experimental procedure

2.1. Coating system preparation

Nickel base alloy bar stock with nominal composition in weight percent of Ni-7Cr-8Co-2Mo-5W-7Ta-3Re-6.2Al-0.2Hf-0.002Y [13] was fabricated into coupons with nominal dimensions of 25.4 mm (1 inch) by 3.18 mm (0.125 inch) diameter. Media finishing of all coupons was done to round the coupon sharp edges and produce a finish similar to media finished production parts.

After machining, each coupon was bond coated with MDC-150L, a chemical vapor deposition (CVD) aluminizing process [14].

Application of the TBC was performed in three TBC runs. One process variable, set at three different levels, was the only processing difference between each run. All runs were performed in PVD1, a developmental physical vapor deposition coater designed with production capability in terms of pre-heater, part manipulation and evaporation characteristics. The ceramic was 7 wt.% yttria stabilized zirconia (7YSZ).

After TBC application, all coupons were heat treated to partial solution and age cycles per the alloy requirements.

2.2. Testing and analysis

2.2.1. Photo-stimulated luminescence spectroscopy

The as-processed and cross-sectioned samples were characterized at ORNL using a Dilor XY800 Raman microprobe (Jobin Yvon Inc.) configured to operate as a single stage spectrograph. The laser was an argon ion laser (Coherent, Inc., Model #308C) operating at 514.5 nm with an output power of 500 mW. An attached microscope focused the incident laser to a spot size of 10–12 μm onto the TBC top surface. A curve fitting routine was used to fit a psuedo-Voigtian curve to the acquired spectra. Using this program, peak shifts as low as ~ 0.01 cm^{-1} were resolvable. The spectra were calibrated using an emission line from the argon ion laser at 696.5 nm. Five spectra from each sample were recorded between 14 300 and 14 700 cm^{-1}. Using techniques developed by Clarke et al. [8–11] several qualities of the TGOs can be compared — residual stress, phases present and thickness.

2.2.2. SEM analyses

SEM analysis was carried out twice. Initially, SEM images of the TGO in the as-deposited TBC condition for each process were made at 5000× and 20 kV using a Topcon DS701 at HRC. Prior to performing the imagining, each sample was cross-sectioned, mounted in Konductmet® mounting compound, and gold sputtered to improve surface electrical conduction and reduce charging of the sample.

A separate portion of each sample described above was analyzed using high resolution (30 000×), low voltage (5 kV) SEM imaging of the as-deposited TBC polished cross-section at ORNL using an Hitachi S4700 FEG/SEM.

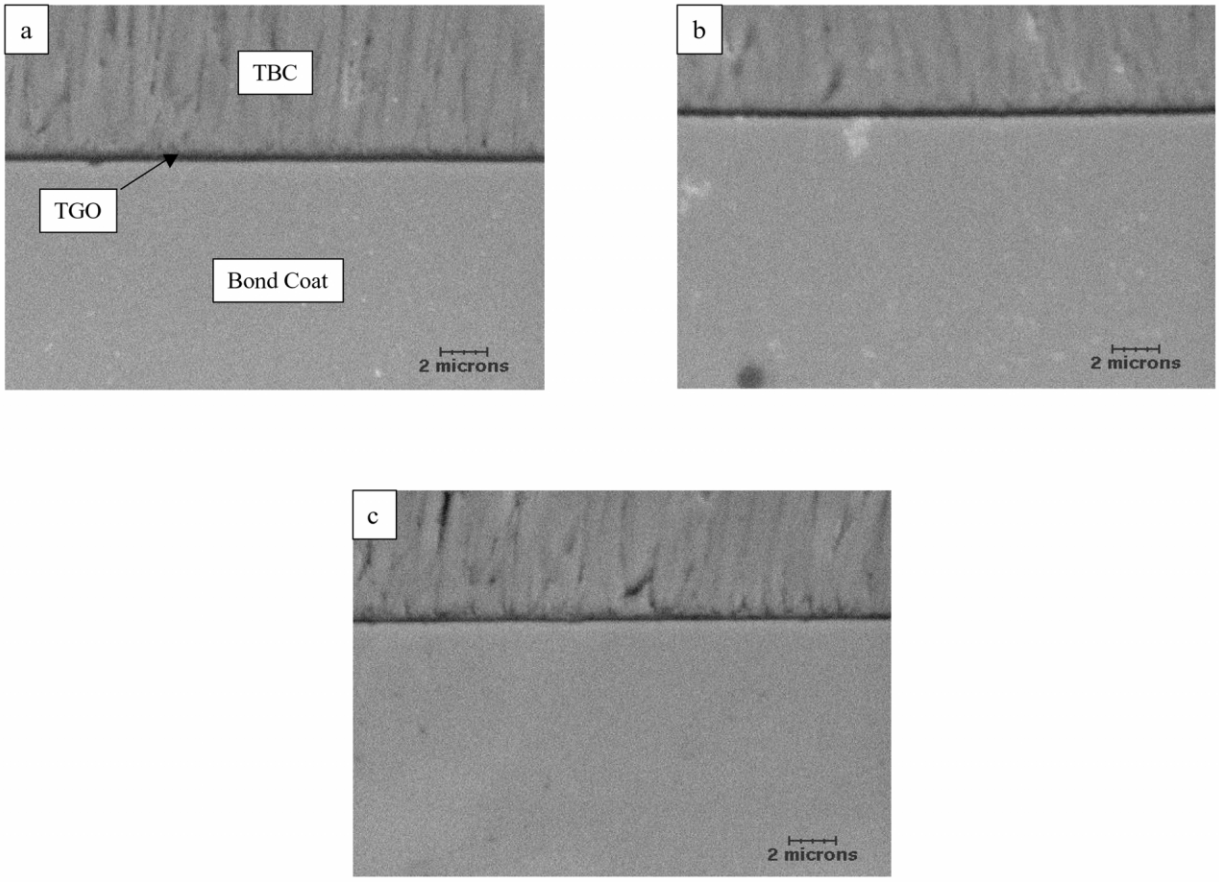

Fig. 1. Typical SEM images of the as-deposited TBC TGO interfacial regions for Process A (a), Process B (b), and Process C (c) at 5000×. Specimens were Au sputtered and examined at 20 kV.

2.2.3. TEM/STEM characterization

The technique for preparing TBC/TGO/(Ni,Pt)Al cross-sections for TEM analysis using the FIB were developed at ORNL. After slices were cut for standard metallographic cross-sections, additional pieces (2 mm×2 mm×2 mm) were cut for TEM cross-section specimen preparation. First, the top ~80–90 μm of the TBC was removed from these specimens. Next, the cross-sectioned samples were mechanically thinned using an Allied High Tech Products, Inc. Techprep Polishing Machine (equipped with Multiprep Micropositioning Head) to ~50 μm thick and mounted on a Be support ring for final thinning to electron transparency using the Hitachi FB-2000A FIB System. The FIB utilizes Ga ions to selectively etch a 20 μm×20 μm thin section from the surface of the specimen for TEM imaging [15]. This uniformly thin 'window' of material (≪0.1 μm) contains all the regions of interest for subsequent TEM/STEM analysis. An FEI/Philips CM200 FEG-STEM equipped with an Oxford superatmospheric thin window energy dispersive spectrometer (EDS) and an EMiSPEC integrated acquisition system for X-ray microanalysis was used for dark-field and bright-field imaging and high resolution elemental mapping of the full TGO interfacial region. A JEOL 4000EX dedicated high resolution TEM was used for atomic structure imaging of the TGO crystalline phases. Diffraction data from the different phases present within the TGO interfacial region were obtained directly from the high resolution images.

3. Results

3.1. TBC morphology/TGO thickness

Fig. 1 shows typical 5000× SEM images of the TBC/TGO/bond coat interfacial region for each process. Note that no distinct TGO microstructural features are observed using this sample preparation method and magnification for any of the samples.

3.2. Photo-stimulated luminescence spectroscopy (PSLS)

The remaining portion of coupons from Processes A, B, and C were measured with PSLS by ORNL prior to

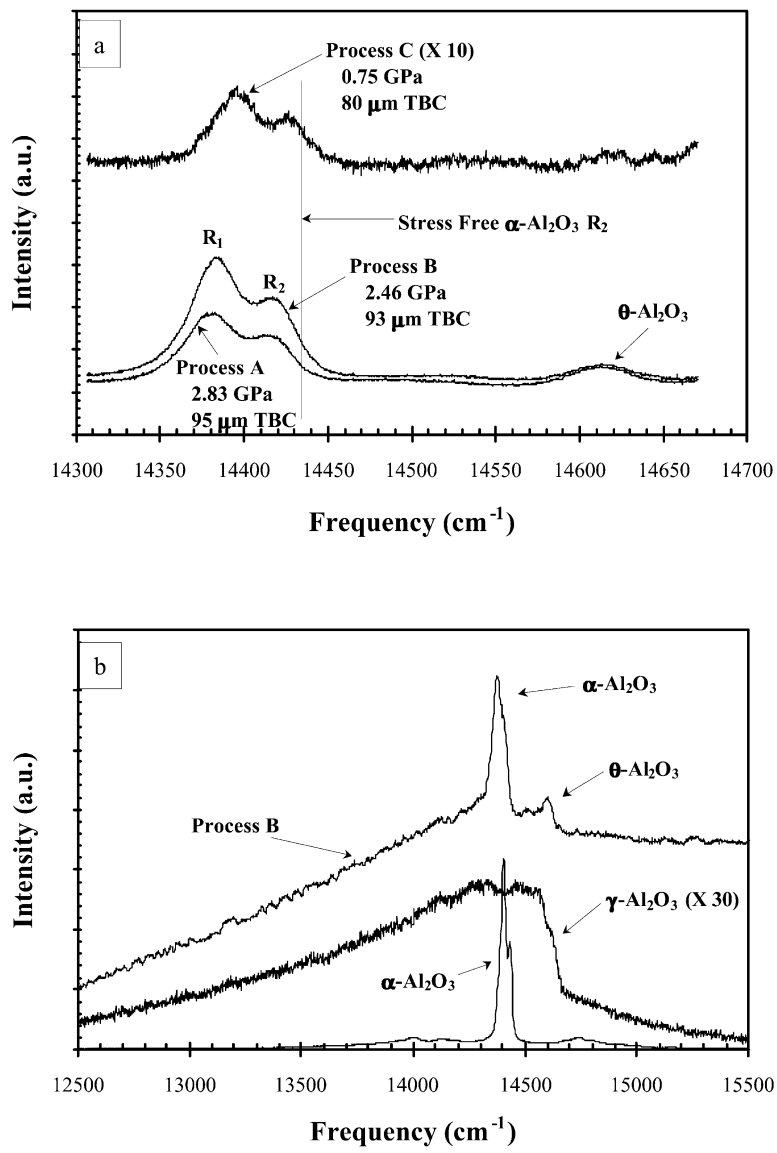

Fig. 2. (a) Photo-stimulated luminescence spectra (PSLS) from TGO of Process A, Process B, and Process C and corresponding TGO residual stress and TBC thickness. (b) PSLS spectra obtained from pure α and γ-Al_2O_3 powders and Process B TGO. The intensity of the spectra from the pure γ-Al_2O_3 powder has been multiplied by 30.

high resolution SEM imaging sample preparation. Fig. 2a shows the spectra from each sample between 14 300 and 14 700 cm^{-1}. Note that the Process C spectrum was magnified 10 times to make the α-alumina R_1 and R_2 peaks observable compared with the other spectra.

In addition to being able to measure stress in α-Al_2O_3, PSLS can detect the presence of θ and γ-Al_2O_3 [10,17]. Fig. 2b shows spectra acquired from pure α and γ-Al_2O_3 powder as well as sample Process B between 12 500 and 15 500 cm^{-1}. In this case, the Process B sample has been cross-sectioned so that the TGO can be inspected directly without interference from the TBC. The luminescence spectra from the α phase is characterized by the two well-known R-lines whereas the γ phase is a broad background with a sharp cut-off starting at ~14 600 cm^{-1}. The γ signal is much weaker than that of α as is reflected by the fact that the intensity of the γ spectra in Fig. 2b has been multiplied 30 times. Also, α-Al_2O_3 has some background luminescence and the YSZ TBC itself may fluorescence somewhat due to being slightly non-stoichiometric.

3.3. High resolution SEM imaging

At higher magnifications, microstructural details within the TGO interfacial region can be resolved. Fig. 3a–c show the TGO in the as-deposited TBC condition for each process. In Processes A and B, a mixed oxide zone

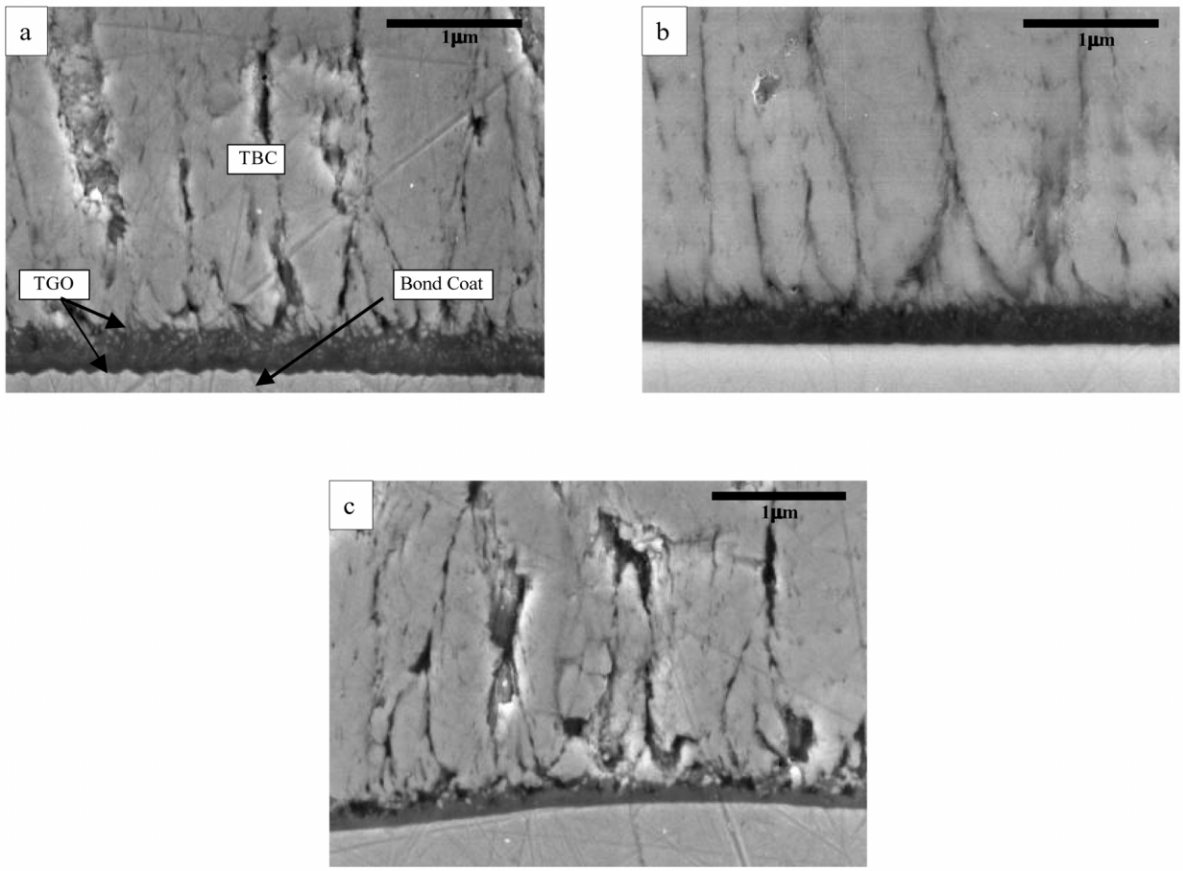

Fig. 3. Typical SEM images of the as-deposited TBC TGO interfacial regions for Process A (a), Process B (b), and Process C (c) at 30 000×. The mixed oxide zone is clearly visible for Processes A and B. Some mixed oxide zone is visible for Process C.

(Al_2O_3 + 7YSZ) is clearly observed above a distinct and continuous oxide layer. In Process C, the mixed oxide zone may also be present, but much thinner and comprised of larger grained 7YSZ.

3.4. STEM compositional analysis

Dark Field STEM images and corresponding Al and Zr high resolution elemental X-ray maps for each process are shown in Figs. 4–6. All three processes show that the TGO consists of a continuous and pure alumina layer between the bond coat and the mixed oxide zone. These three figures also annotate how the TGO is divided into the mixed oxide zone and a continuous Al_2O_3-layer. Table 1 lists the thickness measurements of the mixed oxide zone and the continuous Al_2O_3-layer and the alumina polymorphs detected for this work and Stiger et al. [16] in the as-deposited condition. Additionally, there is substantially more porosity in the Process C mixed oxide zone than in either Process A or B.

Inspection of the X-ray maps shows that the YSZ particle size observed in the mixed oxide zone formed for Process C is much coarser than that observed for Process A or B.

3.5. High resolution TEM imaging and diffraction analyses

High-resolution atomic structure imaging was used to identify the crystalline Al_2O_3 polymorphs present within the TGO region. Numerous high-resolution images were taken from the different areas (continuous layer and mixed oxide zone) of the FIB-prepared specimens representing each of the three Processes (A, B or C). Fast Fourier transforms (FFT) were then taken from several different areas on each image to determine interplanar spacings that would uniquely define the crystallographic structure of the phase being imaged. The FFTs give the periodicities observed in the image area selected, effectively giving the reflections (interplanar spacings) that would be observed in a direct electron diffraction pattern. Yttria-stabilized zirconia particles within the mixed oxide zone were used as the 'internal' standard for the FFT calibration.

This procedure is illustrated in Figs. 7 and 8. Fig. 7 is a relatively low magnification bright field TEM image

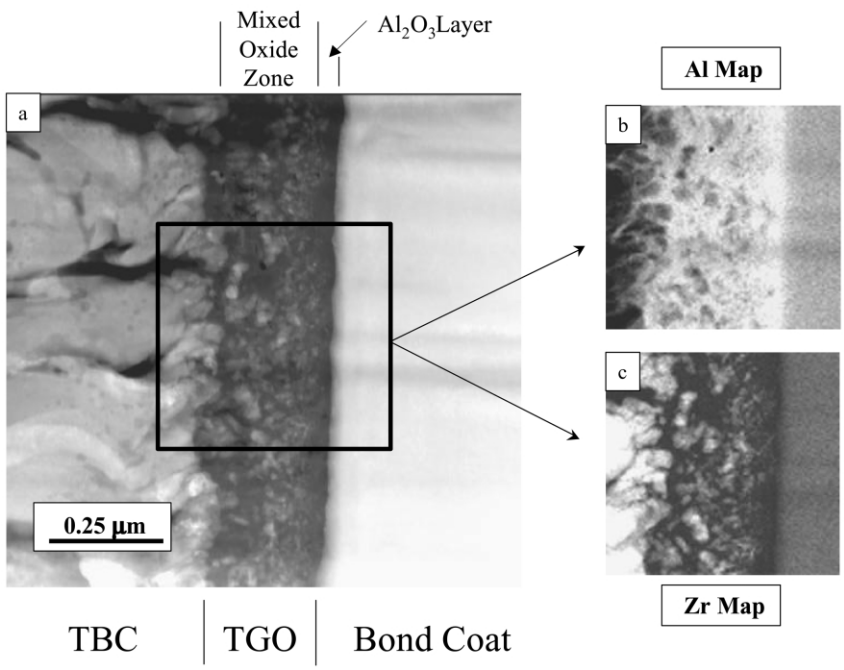

Fig. 4. (a) STEM dark field image and Al (b) and Zr (b) elemental maps of sample produced by Process A. The dark field image has been annotated to show the mixed oxide zone and continuous Al_2O_3 layer of the TGO.

of the continuous alumina layer and mixed oxide zone observed in (Process C). High resolution images were then taken from many selected areas, such as that within the box (in the continuous alumina layer) in Fig. 7. Fig. 8 shows the atomic structure image of the area boxed in Fig. 7 and the corresponding FFT from this localized area. The FFT shows a cubic ⟨112⟩ type pattern indicating that the continuous phase is γ-alumina. In fact, many FFTs were taken from the continuous alumina layer in all three samples and all the FFT data show

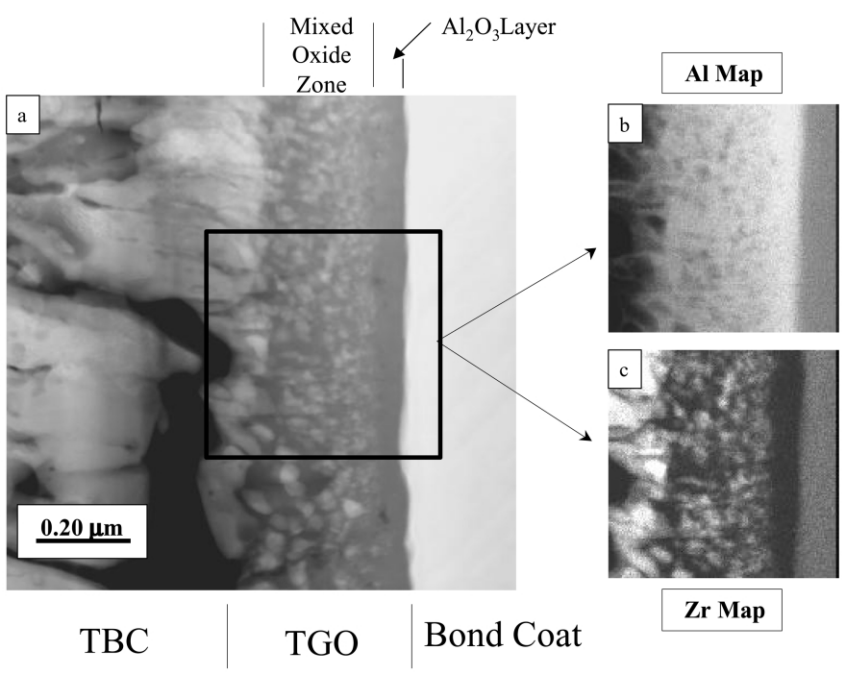

Fig. 5. (a) STEM dark field image and Al (b) and Zr (b) elemental maps of sample produced by Process B. The dark field image has been annotated to show the mixed oxide zone and continuous Al_2O_3 layer of the TGO.

that the continuous layer is single phase γ-alumina in all three samples. FFTs from many particles within the mixed oxide zone from Processes A and B show that the major alumina phase in this region is also γ-alumina with particles of α- and θ-alumina identified and mixed with the YSZ particles. The FFT data from Process C, however, identified γ -alumina as the predominant phase through the entire TGO interfacial region. No particles of either α- or θ-alumina were identified from the high-resolution images. This does not conclude that there is absolutely no α- or θ-alumina within the mixed region (the PSLS data showed that there was some of each phase present), only that neither phase was identified using high-resolution TEM imaging.

4. Discussion

4.1. Initial observations

As seen in Fig. 1, SEM imaging at low magnification (5000×) with a conductive gold film is not sufficient to show the morphological details of the thin TGO nor obtain an accurate measurement for the TGO thickness. Using these images alone (which are typical of the results obtained at industrial production facilities), one might assume that there were no microstructural differences between the TGO regions produced by Processes A, B and C.

Residual stress calculations in the TGO for the different TBC deposition processes are shown in Fig. 2. They are calculated from the R_2 wave number shift relative to stress free α-alumina. The calculations show that Processes A and B resulted in a 2.8- and 2.4-GPa compressive stress, respectively, whereas Process C produced only a 0.8-GPa compressive stress. These stress values suggest that the TGO transformation of the alumina to α-alumina is not complete after all three Processes, with Process C clearly having the least amount of transformation. Depending on surface roughness, complete transformation of the TGO to α-alumina should yield a residual compressive stress in the range 3.3 GPa [18].

Table 1
As-deposited thickness measurements

Coating	Mixed oxide zone layer (μm)	Continuous alumina layer (μm)	Alumina phase(s)
Process A	0.30	0.04	α,θ,γ
Process B	0.29	0.06	α,θ,γ
Process C	0.19	0.04	α,θ,γ
Stiger et al. [16]	None	0.07	α

4.2. Mixed oxide zone is found in all TGO morphologies studied

High magnification, low voltage SEM imaging of polished cross-sections in Fig. 3 reveal the true nature of the individual layers within the thin TGO of the as-deposited TBC. A continuous alumina layer is observed

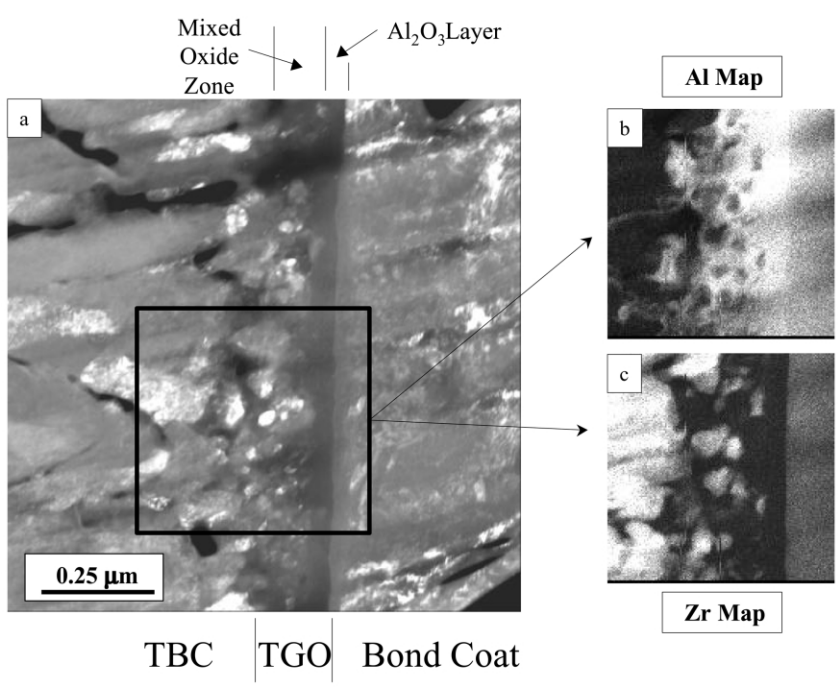

Fig. 6. (a) STEM dark field image and Al (b) and Zr (b) elemental maps of sample produced by Process C. The dark field image has been annotated to show the mixed oxide zone and continuous Al_2O_3 layer of the TGO.

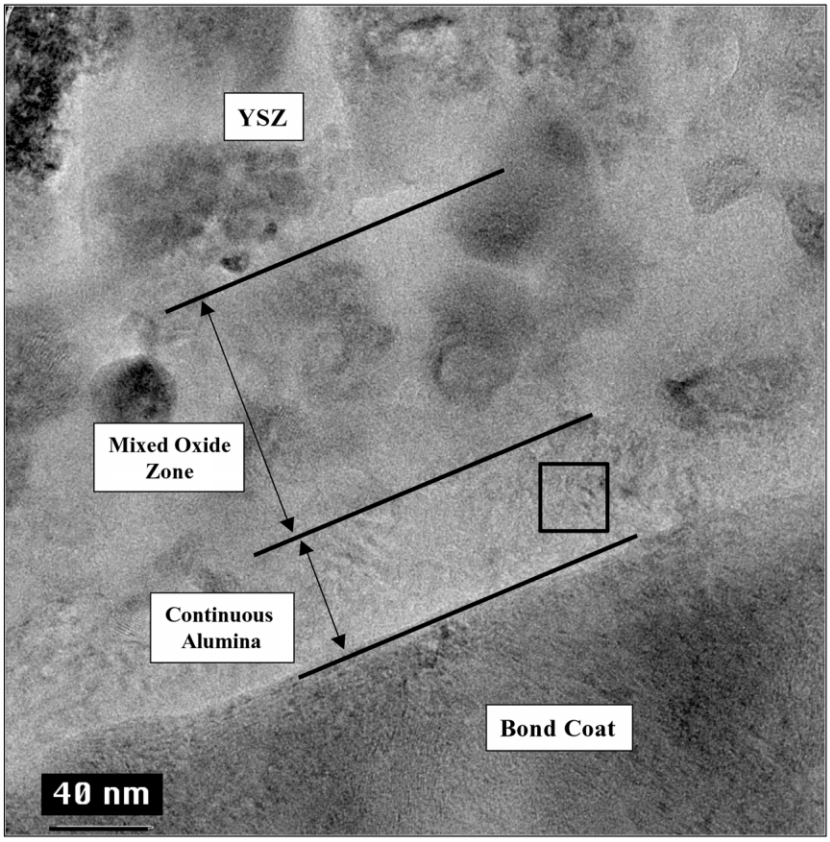

Fig. 7. Bright field image of the TGO interfacial region formed by Process C.

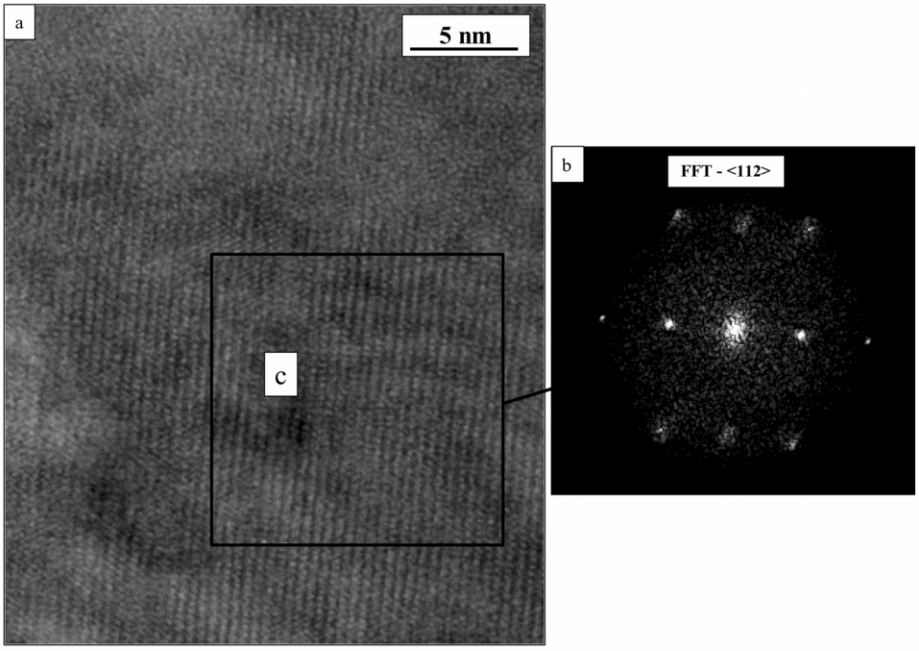

Fig. 8. (a) High-resolution TEM image and (b) corresponding FFT (from area within box on image) from the continuous alumina layer within the TGO interfacial region produced by Process C. The FFT is a cubic ⟨112⟩ type pattern matching γ-alumina. This layer was found on all three processes.

in the cross-sections for all three processes. However, the mixed oxide zone, while clearly present within the TGO region produced by Processes A and B, is observed only to a limited extent in the sample produced by Process C. Also, the total TGO thicknesses resulting from Processes A and B are ~40% thicker than that produced during Process C.

The primary structural difference within the TGO produced by the different processes is clearly within the mixed oxide zone. Processes A and B (Figs. 4 and 5) result in the formation of an extremely fine-grained (< 0.02 μm), relatively thick (~0.3 μm), pore-free Al_2O_3+YSZ layer. The mixed oxide zone in the samples produced by both Process A and B are composed of nano-crystalline γ-, α- and θ-aluminas+YSZ. In contrast, the mixed oxide zone formed during Process C (Fig. 6) has a much larger YSZ grain size (~0.08 μm), is considerably thinner (~0.2 μm), is primarily γ-alumina+YSZ, and contains numerous pores.

4.3. Gamma alumina is the predominate phase in the TGO for all three processes

The dark field STEM images and corresponding high resolution Al and Zr EDS maps shown in Figs. 4–6 for the FIB-produced cross-sections from Processes A, B and C, respectively, provide additional insight into the true morphological variances for the thin TGO regions in the as-deposited TBC samples. The continuous, pure alumina layer is evident in both the STEM images and EDS maps for samples produced by all three processes. Results of high-resolution TEM analyses conclusively show that the predominate phase in all three processes is γ-Al_2O_3. Figs. 7 and 8 illustrate this for Process C. Analysis of the continuous alumina layer showed it is approximately the same thickness and composed of the same single-phase γ-alumina in all three cases. Analysis of many locations within the mixed oxides zone showed only Processes A and B had any evidence for α and θ-Al_2O_3.

The presence of the continuous γ-alumina layer in all three samples and the small amounts of α- plus θ-alumina identified in the mixed oxide zone (identified by TEM) coupled with the residual stress measurements confirm that complete transformation to α-alumina did not occur during any of the processes. In fact, the whole TGO interfacial region (continuous alumina layer plus mixed oxide zone) produced by Process C was composed almost entirely of γ-alumina, which explains the much weaker PSLS spectral intensity and low α-Al_2O_3 residual compressive stress.

4.4. Photo-stimulated luminescence spectroscopy can detect γ-alumina

The TGO from sample Process B was analyzed in cross-section (Fig. 2b) allowing direct measurement of the TGO without interference from the TBC. The R-lines associated with α-Al_2O_3 can be clearly seen as well as those from θ-Al_2O_3. By comparing the shape of the background of this spectrum with that of pure γ-Al_2O_3, it can be seen that γ is present within this sample. The subsequent TEM analysis revealed that the TGO in this sample was predominantly γ-Al_2O_3. This highlights the ability of PSLS to detect γ-Al_2O_3 in addition to θ-Al_2O_3 and α-Al_2O_3. When analyzing as-deposited coatings, the narrow spectral band for accurate measurement of the R_1/R_2 peak shifts and the presence or absence of θ-Al_2O_3, should be augmented with a wide band measurement to determine the presence or absence of γ-Al_2O_3. However, in a through-the-TBC measurement mode, the low signal strength from very thin TGO films may not always allow detection of γ-Al_2O_3.

4.5. Mixed oxide zone formation

A mixed oxide zone has been reported by Stiger [16]. The mixed zone is shown after an air exposure at 1200°C (2192°F). However, recent work has shown that in samples with a grit blasted pre-TBC surface, discontinuous segments of a mixed oxide zone may form in the as-deposited condition.

This work suggests that, during the formation and transformation of the TGO, conditions exist to form a continuous γ-Al_2O_3 layer (Process A, B and C). Process parameters can be adjusted to cause outward growth of the γ-layer and initial conversion to the θ- and α-Al_2O_3 phases (Processes A and B). The outward growth is irregular, not planar in nature. As the TBC is deposited onto this TGO, the 7YSZ fills in the gaps in the irregular TGO morphology creating the mixed oxide zone (γ-, θ-, α-aluminas and 7YSZ).

Upon high temperature exposure, it is predicted that the γ-phase will rapidly transform through the metastable θ-polymorph to the α-phase. It is believed that the α-phase will then grow by predominately inward diffusion of oxygen [19]. As this transformation completes, the continuous γ-Al_2O_3 layer becomes continuous α-Al_2O_3 with compressive stresses in the 3.5–4.0 GPa range and a complex stress state similar to that illustrated by Tolpygo [10] for θ-Al_2O_3 needles grown from continuous θ-Al_2O_3 that then transform to α-Al_2O_3.

5. Conclusions

With proper pre-TBC processing, the formation of a mixed oxide zone within the TGO is possible in as-deposited TBCs. The development of this zone is also affected by pre-TBC processing (surface finishing) as well as PVD deposition conditions.

In all the as-deposited TBCs in this study, the TGO consists of two sub-layers; (1) a continuous layer of γ-Al_2O_3 between the mixed oxide zone and the bond coat; and (2) a mixed oxide zone between the continuous γ-Al_2O_3 and the TBC layer.

Process parameters can be adjusted to cause outward growth of the γ-layer and initial conversion to the θ- and α- Al_2O_3 phases (Processes A and B). The outward growth is irregular, not planar in nature.

As the TBC is deposited onto this TGO, the 7YSZ fills in the gaps in the irregular TGO morphology creating the mixed oxide zone (γ-, θ-, α-aluminas and 7YSZ).

Acknowledgements

The authors gratefully acknowledge the supportive work by K.S. Trent, D.W. Coffey and T.S. Geer at ORNL for preparing the TEM specimens and performing the SEM imaging. We also thank Professors Meier and Clarke and Dr. Tolpygo for technical discussions regarding this work. This research was also sponsored by the Assistant Secretary for Energy Efficiency and Renewable Energy, Office of Transportation Technologies, as part of the High Temperature Materials Laboratory User Program, Oak Ridge National Laboratory, managed by UT-Battelle, LLC, for the US Department of Energy under contract number DE-AC05-00OR22725. M.J. Lance supported in part by the Division of Materials Sciences and Engineering, Office of Basic Energy Sciences, Department of Energy.

References

[1] R.A. Miller, Thermal Barrier Coating Workshop NASA Conference Publication 3312, Cleveland, OH, USA, 1995, p. 17.
[2] S. Bose, J. DeMasi-Marcin, Thermal Barrier Coating Workshop NASA Conference Publication 3312, Cleveland, OH, USA, 1995, p. 63.
[3] J.R. Nicholls, Y. Jaslier, D.S. Rickerby, Mater. High Temp. 15 (1) (1998) 15.
[4] J.R. Nicholls, M.J. Deakin, D.S. Rickerby, Wear 233–235 (1999) 352.
[5] T. Strangman, US Patent #4,321,311 (1982).
[6] N. Ulion, US Patent #4,321,310 (1982).
[7] J.C. Schaeffer, Thermal Barrier Coating Workshop Sponsored by the TBC Interagency Coordination Committee, 1997, p. 99.
[8] R.J. Christensen, D.M. Lipkin, D.R. Clarke, K.S. Murphy, Appl. Phys. Lett. 69 (24) (1996) 3754.
[9] P. Peng, D.R. Clarke, J. Am. Ceram. Soc. 83 (5) (2000) 1165.
[10] V.K. Tolpygo, D.R. Clarke, Mater. High Temp. 17 (1) (2000) 59.
[11] N.E. Paton, K.S. Murphy, D.R. Clarke, US Patent #6,072,568 (2000).
[12] K.L. More, D.W. Coffey, B.A. Pint, K.S. Trent, P.F. Tortorelli, Proc. Microsc. Microanal. 2000 6 (2) (2000) 540–541.
[13] G.L. Erickson, Adv. Mater. Process. (1997) 29.
[14] B.M. Warnes, ASME International Gas Turbine & Aeroengine Congress & Exhibition, Stockholm, Sweden, 98-GT-391.
[15] V. Dravid, Hitachi Instrum. News 34 (1998) 3.
[16] M.J. Stiger, N.M. Yanar, F.S. Pettit, G.H. Meier, in: J.M. Hampikian, N.B. Dahotre (Eds.), Elevated Temperature Coatings: Science and Technology III, The Minerals, Metals & Materials Society, San Diego, CA, 1999, p. 51.
[17] D.M. Lipkin, H. Schaffer, F. Adar, D.R. Clarke, Appl. Phys. Lett. 70 (19) (1997) 2250.
[18] D.M. Lipkin, D.R. Clarke, M. Hollatz, M. Bobeth, W. Pompe, Corrosion Sci. 39 (1997) 231.
[19] K.M.N. Prasanna, A.S. Khanna, R. Chandra, W.J. Quadakkers, Oxidat. Metals 46 (5/6) (1996) 465.